Food Hydrocolloids 137 (2023) 108291

Contents lists available at ScienceDirect

Food Hydrocolloids

journal homepage: www.elsevier.com/locate/foodhyd

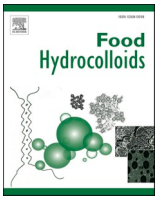

Emulsifying properties of sugar beet pectin microgels

Samuel J. Stubley [a], Olivier J. Cayre [b], Brent S. Murray [a,*], Isabel Celigueta Torres [c]

[a] Food Colloids & Bioprocessing Group, School of Food Science & Nutrition, University of Leeds, UK
[b] Colloid and Polymer Engineering Group, School of Chemical & Process Engineering, University of Leeds, UK
[c] Nestlé Product Technology Centre Confectionery, York, UK

ARTICLE INFO

Keywords:
Emulsions
Pectin
Microgel
Laccase
Sugar beet
Rheology

ABSTRACT

Particle stabilized ('Pickering') oil-in-water (*O/W*) emulsions were fabricated using sugar beet pectin (*SBP*) microgel particles (*SBPM*) that differed in their crosslinking density and therefore elasticity. Droplet size distributions and emulsion microstructures were investigated via light scattering and complimentary imaging techniques: light microscopy, confocal laser scanning microscopy and scanning electron microscopy. Comparisons to emulsions stabilized by native (*i.e.,* non-microgelled) *SBP* at equivalent overall *SBP* content were made throughout. The *SBPM*-stabilized emulsions (20 and 40 vol% oil) were shown to have an improved physical stability compared to those stabilized by *SBP*. For example, droplet coarsening on prolonged (9 week) storage at ambient temperature (25 °C) and on temperature cycling (75 °C) was substantially reduced for *SBPM*-stabilized emulsions. This is attributed to the greater steric barrier provided by *SBPM* particles and their higher energy of displacement. Furthermore, the higher viscoelasticity of the *SBPM*-stabilized emulsions (particularly at 40 vol% oil) retarded droplet creaming. This higher viscoelasticity could be due to weak flocculation of the *SBPM*-stabilized droplets or the strong influence of the *SBPM* on the viscoelasticity of the intervening aqueous phase, even at relatively low *SBPM* concentrations.

1. Introduction

Pectin is a heteropolysaccharide extracted from plant cell walls with a chemical structure dependent on the plant source and extraction conditions. The main structural component, Homogalacturonan (*HG*), is essentially a linear polymer of galacturonic acid (*GalA*) where some of the *GalA* residues may be methylated or acetylated. The second major structural region is Rhamnogalcturonan I (*RGI*), whose backbone consists of *GalA* interspersed with rhamnose residues. Branching from the main chain occurs in the form of neutral sugar side chains composed mainly of arabinose and galactose residues (Ngouémazong, Christiaens, Shpigelman, Van Loey, & Hendrickx, 2015; Thakur, Singh, Handa, & Rao, 1997). In addition, protein has frequently been observed in some extracted pectins, including sugar beet pectin (*SBP*), although the origin, location and distribution of such proteinaceous elements is currently not entirely clear. The key point is that such protein elements confer surface activity on these pectins, allowing for their use as emulsifiers, as reviewed elsewhere (Alba & Kontogiorgos, 2017; Ngouémazong et al., 2015). At the same time, the non-surface active polysaccharide elements confer excellent electrosteric stability by protruding into the aqueous continuous phase of oil-in-water (*O/W*) emulsions (Akhtar, Dickinson, Mazoyer, & Langendorff, 2002; Dickinson, 2003). *SBP* tends to contain more protein and also a greater proportion of acetyl groups (Leroux, Langendorff, Schick, Vaishnav, & Mazoyer, 2003; Schmidt, Schmidt, Kurz, Endreβ, & Schuchmann, 2015) compared to other commonly utilized pectins from apple and citrus sources and their emulsifying properties have been studied in some detail. The acetyl groups are believed to increase the hydrophobicity and therefore the surface activity of the *SBP* (Dea & Madden, 1986). Indeed, synthetic acetylation of depolymerized citrus pectins improved their performance as emulsifiers, enabling the stabilization of finer O/W emulsion droplets (Leroux et al., 2003). The measured proportion of protein associated with *SBP* seems to vary greatly between studies, probably due to differences in the extraction conditions (Chen et al., 2016; Yapo, Robert, Etienne, Wathelet, & Paquot, 2007). Atomic force microscopy studies have confirmed that the protein is directly attached to the polymer backbone - approximately 66% of the imaged *SBP* molecules contained protein (Kirby, MacDougall, & Morris, 2006). This is in agreement with previous observations that pectins adsorb to *O/W* interfaces via their protein-rich fractions (Akhtar et al., 2002; Leroux et al., 2003; Siew & Williams,

* Corresponding author.
E-mail address: b.s.murray@leeds.ac.uk (B.S. Murray).

https://doi.org/10.1016/j.foodhyd.2022.108291
Received 12 August 2022; Received in revised form 14 October 2022; Accepted 2 November 2022
Available online 10 November 2022

2008; Williams et al., 2005) and that treatment of *SBP* with proteases significantly decreases their performance as emulsifiers (Chen et al., 2016; Funami et al., 2007).

Another significant feature of *SBP* is the presence of ferulic acid residues esterified to the neutral sugar side chains of the *RGI* regions (Levigne et al., 2004). While ferulic acid has been suggested as also increasing the *SBP* hydrophobicity and surface activity (Siew, et al., 2008; Williams et al., 2005), it also makes the *SBP* susceptible to chemical crosslinking via oxidative coupling reactions. Oxidation of ferulic acid can be catalyzed by persulphates (Thibault, Garreau, & Durand, 1987) or oxidoreductase enzymes, resulting in the generation of phenoxy radicals. Radical coupling leads to *SBP* molecules that are cross-linked via ferulic acid dimers and/or higher ferulate oligomers (Bunzel, 2010).

Such oxidative crosslinking has been exploited to improve the stability of *SBP*-stabilized emulsions by crosslinking the *SBP* molecules in dilute solution prior to their use as emulsifiers. For example, *SBP* has been cross-linked via laccase (Jung & Wicker, 2012) and horseradish peroxidase (L. Zhang et al., 2015). In each case, the increase in the *SBP* molecular weight (M_W), as confirmed by size exclusion chromatography, led to emulsions with improved storage stability compared to the native *SBP*. This was attributed to the development of a thicker and more viscoelastic film adsorbed at the interface, which was more effective at reducing droplet coalescence.

Another interesting use of oxidative crosslinking of *SBP* is in the preparation of chemical hydrogels (Thibault et al., 1987) which are thermally irreversible (Khalighi, Berger, & Ersoy, 2020) and resist dissolution when placed in excess solvent (Stubley, Cayre, Murray, Torres, & Farrés, 2021). We recently exploited this technique to prepare sugar beet pectin microgels (*SBPM*), by homogenizing bulk *SBP* hydrogels (cross-linked via laccase) in the presence of excess solvent (water) to produce aqueous suspensions of microgel particles (Stubley, Cayre, Murray, & Torres, 2022; Stubley et al., 2021). Microgels are solvent swollen polymer networks of finite dimensions, a type of soft colloid demonstrating the properties of both polymers and particles (Dickinson, 2016; Lyon & Fernandez-Nieves, 2012). In general, microgel suspensions appear to be very promising for bulk rheology modification, as an alternative to polymer solutions (Adams, Frith, & Stokes, 2004; Stubley et al., 2022; Stubley et al., 2021). However, since *SBP* is surface active, it might be expected that *SBPM* would also be surface active and testing the ability of *SBPM* to stabilize *O/W* emulsions is the main topic that this paper seeks to address.

The use of biopolymer-based microgels as particulate ('Pickering') stabilizers of emulsions, foams, *etc*. has been reviewed extensively elsewhere (Dickinson, 2015; Murray, 2019). In general, they are thought to provide superior stability to coalescence and Ostwald ripening, via the general Pickering mechanism of strong and irreversible adsorption of the particles to the interface, whilst their large size (larger than the polymer molecules of which they are composed) provides a thicker steric barrier. In addition, the particle-stabilized systems may provide extra benefits such as reduction of oil oxidation (Atarés, Marshall, Akhtar, & Murray, 2012; Kargar, Fayazmanesh, Alavi, Spyropoulos, & Norton, 2012) and of lipid digestion rate (Sarkar, Zhang, Holmes, & Ettelaie, 2019), depending on the nature of the stabilizing particles.

There are several recent publications on the use of polysaccharide based microgels to stabilize emulsions (Hu et al., 2021; Huang et al., 2021; Ishii, Matsumiya, Aoshima, & Matsumura, 2018; Lefroy, Murray, Ries, & Curwen, 2021) including other pectin based microgels. For example, Mironov et al. (2013) used a "bottom-up" approach to microgelation in dilute solution. Their synthesis involved chemical crosslinking of pectinic acid via a basic isocyanide and amine leading to the development of polyampholyte microgels which precipitated around their pI. Stable emulsions could be prepared at low pH, where particles were strongly positively charged, while emulsions could be broken by raising the pH > pI (Mironov, Shulepov, Ponomarev, & Bakulev, 2013). However, the use of such chemicals and the organic solvents utilized in their synthesis probably make such microgels unsuitable for use in food and drinks. Also, Saavedra Isusi and coworkers have published a series of papers (Saavedra Isusi, Bindereif, Karbstein, & van der Schaaf, 2020; Saavedra Isusi, Lohner, Karbstein, & van der Schaaf, 2021; Saavedra Isusi, Madlindl, Karbstein, & van der Schaaf, 2020; Saavedra Isusi, Weilandt, Majollari, Karbstein, & van der Schaaf, 2021) investigating the emulsifying properties of low methyl ester pectin microgels, which are physically cross-linked by divalent calcium ions and that may be promising for stabilizing emulsions where biocompatibility is important. Building on these previous works, the chemical crosslinking mechanism exploited in the study reported here yields robust microgel particles whilst maintaining biocompatibility.

Taking inspiration from the debate in the literature as to whether 'softer' or 'harder' microgels give better emulsion stability (Murray, 2019), this work studies the *O/W* emulsion stabilizing properties of two sets of *SBPM*, which differed in their crosslinking density. We investigate the physical stability of *SBPM* stabilized emulsions towards droplet coarsening and phase separation on prolonged storage (9 weeks) at 25 °C and on temperature cycling to 75 °C making comparisons to native (*i.e.,* non-cross-linked) *SBP* stabilized emulsions throughout. Complementary imaging techniques and rheological characterization were used to explain the factors which promote long term stability.

2. Materials and methods

2.1. Materials

Sugar beet pectin (GENU® Beta Pectin) (*SBP*) was a gift from CP Kelco (Lille Skensved, Denmark). Laccase Y120 (EC 1.10.3.2) was obtained from Amano Enzyme (Nagoya, Japan). Type I (Milli-Q) water (Millipore, Bedford, UK) with a minimum resistivity of 18.2 MΩ cm^{-1} was used throughout. Fluorescein isothiocyanate-dextran (*FITC*-dextran, average $MW = 2 \times 10^6$ Da), Nile Red and *n*-tetradecane were obtained from Sigma Aldrich (Dorset, UK).

2.2. Preparation of SBP solutions

SBP powder was dispersed into cold water via a T25 ULTRA-TURRAX blender (IKA, Oxford, UK) equipped with an S25N - 18G dispersing tool at a speed of 15,000 rpm. The powder was added gradually to prevent clumping and the resulting stock solutions were stirred magnetically for a minimum of 12 h in sealed Duran® bottles. The *SBP* solutions were then centrifuged (Eppendorf 5810 R, Stevenage, UK) at 4000 rpm for 60 min in approximately 30 ml aliquots to remove any remaining insoluble material. The supernatant was carefully decanted and stored in sealed containers prior to further use.

The total *SBP* concentration in the supernatants, referred to as C_{PTOTAL} throughout, was determined by drying the purified solutions in a vacuum oven (Townson and Mercer Limited, Croydon, England) at 75 °C and a pressure of 600 mm Hg until no change in mass was observed. To allow for a direct comparison between the emulsifying properties of native (*i.e.,* non-cross-linked) *SBP* and *SBPM*, solutions or suspensions were diluted to the same $C_{PTOTAL} = 0.5$ wt%.

2.3. Fabrication of SBP hydrogels and SBPM suspensions

Laccase stock solutions were prepared by solubilizing the enzyme powder in water for a minimum of 20 min. Subsequently, 5 ml laccase was combined with 25 ml *SBP* stock solution via vortex mixing to give a final enzyme concentration of 0.1 mg ml^{-1} laccase. When the two solutions were visibly well mixed, 'parent' hydrogels were allowed to develop quiescently in sealed containers for a minimum of 12 h by incubation at 25 °C. The elasticity of *SBP* hydrogels depends strongly on the *SBP* concentration in the gel (C_{GEL}) (Stubley et al., 2021). In this work, we have chosen to refer to the hydrogels, plus the microgels derived from them, as 'soft' when $C_{GEL} = 2.4$ wt% and 'firm' when C_{GEL}

= 4 wt%. The development and rheology of these gels has been described in detail earlier (Stubley et al., 2021) and these designations of soft and firm are based on yield stress and strain values of 84% and 460 Pa for C_{GEL} = 2.4 wt% and corresponding values of 63% and 853 Pa for C_{GEL} = 4 wt%. (These values were obtained in strain amplitude sweep tests at an angular frequency of 3.14 rad s^{-1}, performed as described in section 2.9 below, i.e., as for measurements on emulsions).

For the fabrication of the *SBPM* suspensions, the parent hydrogels were broken into coarse lumps with a metal spatula and 25 g of the parent hydrogel were combined with 100 g of deionized water and blended via the ULTRA-TURRAX at 10000 rpm for 10 min. To account for any losses during sample preparation, C_{PTOTAL} of any (*SBPM*) suspensions used as emulsifier was determined by drying the suspensions as described above for the *SBP* supernatants.

2.4. Fabrication of oil-in-water (O/W) emulsions

Tetradecane (ρ = 0.76 g cm^{-3}) was used as the dispersed phase in the fabrication of *O/W* emulsions at oil volume fractions (ϕ_{oil}) of 20 or 40%, to avoid complications from competing surface-active species present in other oils such as vegetable oils. For the continuous phase, *SBP* solutions or suspensions of the soft or firm *SBPM* were used at an overall C_{PTOTAL} = 0.5 wt%. Emulsions were prepared in 100 ml batches. Coarse emulsions were prepared by combining the oil and aqueous phases in the ULTRA-TURRAX at 18,000 rpm for 2 min. Fine emulsions were prepared immediately afterwards by passing the coarse emulsions through a high pressure jet homogenizer once at 300 bar. Emulsions were mixed gently with a vortex mixer, decanted into sealed containers and incubated at 25 °C until further use. Sodium azide (0.005 wt%) was added as a preservative. In one set of experiments, the *SBPM* suspensions prepared in Methods section 2.3 were separately subjected to the same mechanical treatment used to prepare the fine emulsions, *i.e.,* the combination of both ULTRA-TURRAX shearing and jet homogenization. This microgel suspension is referred to as the 'fine' *SBPM* in the text. This experiment was conducted to understand how the *SBPM* particle size might be further affected by the emulsification conditions.

2.5. Particle size analysis of SBPM and O/W emulsions

A Mastersizer 3000 equipped with the Hydro EV wet sample dispersion unit (Malvern Instruments, Worcestershire, UK) was used to investigate the particle size distributions (*PSD*) of *SBPM* suspensions and emulsions. Samples were dispersed in pure water (20 °C) in the stirred measurement cell of the Mastersizer until the laser obscuration reached >1%. A stirrer speed of 2500 rpm was used throughout. In the Mastersizer *PSD*s are automatically calculated via the manufacturer software from the angular dependence of scattered light intensity via the Mie theory assuming particles are spherical. Mean values of particle diameter, namely the Sauter (surface weighted) mean diameter ($D_{3,2}$) and the volume weighted mean diameter ($D_{4,3}$) are calculated according to:

$$D_{a,b} = \frac{\sum n_i D_i^a}{\sum n_i D_i^b} \quad (1)$$

: where n_i is the number of particles of diameter D_i. From the volume distributions, the width of the distribution was assessed by the D_{10}, D_{50} and D_{90} values, where subscripts correspond to the percentage of particles in a distribution. For example, the D_{50} is the median droplet size: 50% of the particles in a distribution are larger than this and 50% are smaller. Similarly, the 90th percentile gives the diameter of which 90% of the particles in a distribution are smaller.

2.6. Microscopy of SBPM and O/W emulsions

Light microscope (Nikon SMZ-2T, Japan) images were collected with a digital camera (Leica MC120 HD). Emulsions were diluted with water and gently vortex mixed before being transferred to welled glass slides and covered with a cover slip. Microscopy was performed using a 10x objective lens.

A Zeiss confocal laser scanning microscope (*CLSM*) (Model LSM 700, Carl Zeiss Microscopy GmbH, Jena, Germany) equipped with a 20x/0.8 NA objective lens was used. Samples were transferred *undiluted* into welled slides for imaging. To image *SBPMG* suspensions, a reverse contrast was employed whereby the continuous phase (water) was stained using a high molecular weight (*MW*) fluorescein isothiocyanate-dextran (*FITC*-dextran average *MW* = 2 × 10^6 Da), added directly to suspensions at a concentration of 0.1 wt% with mild stirring for 1 h in the dark. The excitation and emission wavelengths (λ) used were λ = 488 and 528 nm respectively. For the emulsions, the oil soluble stain Nile Red (0.4 mg mL^{-1}) was dissolved in ethanol and this stain solution was added at 1 v/v % to the emulsions. Stained emulsions were stirred for 2 h in the dark before imaging by *CLSM*. The excitation and emission wavelengths used for Nile Red were λ = 488 and 561 nm respectively. Images were processed using ImageJ software.

Cryogenic-scanning electron microscopy (*CRYO-SEM*) was performed on freshly prepared, undiluted 40 vol% emulsions over numerous length scales. The instrument used was a Helios G4 CX (FEI, Oregon, USA). The microscope was operated at 2 kV and a working distance of 6.4–8 mm. Emulsions were deposited into hollow copper rivets and rapidly frozen by dipping into liquid nitrogen slush (−180 °C) before being transferred to the *SEM* vacuum chamber. Samples were fractured and imaged at −135 °C without the need for sublimation or sputter coating with metal.

2.7. Stability of O/W emulsions to temperature cycling

The thermal stability of emulsions stabilized by *SBP* and *SBPM* was investigated by subjecting the emulsions to two consecutive heating and cooling cycles. 20 ml of freshly prepared emulsion was transferred to a plastic Falcon tube and placed in a water bath pre-heated to 75 °C for 30 min. Samples were then cooled by placing the tubes in a separate water bath set to 25 °C for an additional 30 min. An aliquot (5 ml) of each emulsion was removed for investigation via laser diffraction and light microscopy before the samples were subjected to a second heating and cooling cycle under the same conditions. Light microscopy and particle size analysis of the heat-cycled emulsions was performed within 1 h of heating.

2.8. Creaming stability of O/W emulsions

Emulsions were transferred into matching glass vials to obtain an emulsion height of approximately 60 mm. Vials were sealed and incubated at 25 °C until required for measurement of creaming stability. Periodically, over the space of 9 weeks, the serum layer height (*i.e.,* the aqueous continuous phase) was measured at three predefined points via a pair of calipers and the average serum layer height recorded. The creaming index (*CI*) was calculated according to:

$$CI\ (\%) = 100 \times \left(\frac{H_s}{H_e}\right) \quad (2)$$

: where H_s is the height of the serum layer below the cream layer and H_e is the total height of the emulsion.

2.9. Shear rheometry of O/W emulsions

An Anton Paar MCR 302 (Anton Paar GmbH, Graz, Austria) rheometer was used for all shear rheology experiments and the raw data were analyzed in the RheoCompass software. All rheological tests were performed using a 50 mm stainless steel parallel plate measuring set, with the gap set to 0.5 mm. As a precautionary measure to prevent wall slip, the measuring set was roughened by gluing water-resistant silicon

carbide sandpaper (600 grit, from 3 M) to both the upper and lower plates with multi-purpose silicone rubber sealant (Dow Corning 732), followed by curing for a minimum of 12 h before use. During rheological characterization, the measuring set was covered with a custom made solvent hood lined with dampened paper towel to minimize solvent evaporation. All emulsions were pre-sheared at a shear rate of 50 s^{-1} for 30 s and left at rest for 10 min before commencing the experiments. The pre-shear, rest and measuring intervals were all performed at 20 °C.

Rotational shear rheometry was conducted in triplicate using a new sample loading for each run. Logarithmic sweeps through shear rate were performed using 5 measuring points per decade and a maximum measuring point duration of 2 min. For oscillatory shear rheometry experiments, the measurement point duration was set to automatic using steady state sensing. Strain (γ) amplitude sweeps were conducted in triplicate using a new sample loading for each run. All γ sweeps were performed at an angular frequency (ω) of 3.14 rad s^{-1}. Frequency sweeps are based on single measurements and were performed at γ within the linear viscoelastic region (*LVER*).

2.10. Statistical analysis

The mean particle size distributions and standard deviations of individual samples, either (i) freshly prepared emulsions (ii) emulsions after storage for 63 days or (iii) emulsions after one or two heating cycles respectively were analyzed in the Minitab software using the one way analysis of variance and students T-test at a significance level of $p < 0.05$.

3. Results and discussion

3.1. PSD and microstructure of SBP- versus SBPM-stabilized emulsions

Fig. 1A shows the *PSD*s of the soft and firm *SBPM* after their initial preparation. The firm microgels demonstrated a Gaussian *PSD* with particle sizes between 20 and 100 μm, whereas the soft microgels showed a bimodal *PSD*. For the latter, the main peak was in a slightly lower size regime: 7–70 μm with a second peak at a significantly lower size of around 1 μm. We have previously suggested that this smaller size fraction may represent some *SBP* aggregates liberated from the parent *SBP* hydrogels during their conversion to *SBPM* suspensions (Stubley et al., 2021).

Note the calculation of the *PSD*s assumes that the particles are spherical. However, the inset in Fig. 1A clearly suggests that the *SBPM*s (in this case the firm ones) have highly irregular morphologies when imaged by *CLSM*. However, the particle sizes in the images seem to be in agreement with the range of sizes in the *PSD*s. In accordance with previous studies on the production of polysaccharide microgels via 'top-down' techniques, differences in average particle size result from the elasticity of the parent hydrogels. Those hydrogels with higher elastic modulus and/or yield stress tend to result in larger particle sizes when fragmented to microgel particles (Ellis & Jacquier, 2009; Saavedra Isusi, Karbstein, & van der Schaaf, 2019; Stubley et al., 2021).

These 'coarse' *SBPM* suspensions were subsequently used as Pickering stabilizers of the *O/W* emulsions. However, in preparing the emulsions, the *SBPM*s were subjected to a further mechanical disruption, more substantial than that used to prepare the *SBPM*s in the first place. The size of stabilizing particles is expected to influence the extent of interfacial coverage and thus the size of the resulting oil droplets (Destribats, Eyharts, et al., 2014). Therefore, the *SBPM* were subjected to the emulsion homogenization conditions *in the absence of oil* and the *PSD* re-measured (as described in the Methods). Fig. 1B shows the *PSD* of these fine *SBPM* dispersions. A clear shift to smaller particle sizes was observed for both the soft and firm *SBPM*, with the main peak in each case shifted to between *ca.* 0.3 and 3 μm. The peak at larger particle sizes is presumed to result from a fraction of particles that survive this additional mechanical disruption, since it appears to correspond to the main peak prior to these 'emulsification' conditions (see Fig. 1A).

Table 1 shows the average particle sizes calculated from the laser diffraction measurements on coarse and fine *SBPM*s. Irrespective of how the average is calculated, it was found to be lower for the fine particles, as expected. For example, $D_{3,2}$ and $D_{4,3}$ decreased from 44.7 to 52.4 μm to 1.3 and 7.2 μm, respectively, for the firm *SBPM*s and from 4.9 to 23.2 to 1.0 and 2.8 μm, respectively, for the soft *SBPM*s.

Measurement of the emulsion *PSD*s requires considerable dilution in the measurement cell in order to obtain a laser obscuration in the correct range. Fig. 2A–C shows the evolution of mean particle size with time after dispersing the 40 vol% *O/W* emulsions stabilized by native *SBP*, the soft and the firm *SBPM*, respectively, into the measurement cell. For the

Table 1
Average particle sizes of coarse and fine *SBPM* particles of different particle elasticity. Firm and soft *SBPM*s were obtained from parent hydrogels prepared at C_{GEL} = 4 wt% and 2.4 wt%, respectively.

Size parameter /μm	Firm coarse	Firm fine	Soft coarse	Soft fine
$D_{3,2}$	44.8 ± 0.1	1.3 ± 0.0	4.9 ± 0.20	1.0 ± 0.0
$D_{4,3}$	52.5 ± 0.2	7.2 ± 0.4	23.2 ± 0.2	2.8 ± 0.1
D_{90}	82.1 ± 0.4	26.6 ± 1.2	43.3 ± 0.1	3.0 ± 0.2
D_{50}	49.2 ± 0.1	1.3 ± 0.0	22.5 ± 0.2	1.0 ± 0.0
D_{10}	28.2 ± 0.2	0.6 ± 0.0	1.2 ± 0.0	0.6 ± 0.0

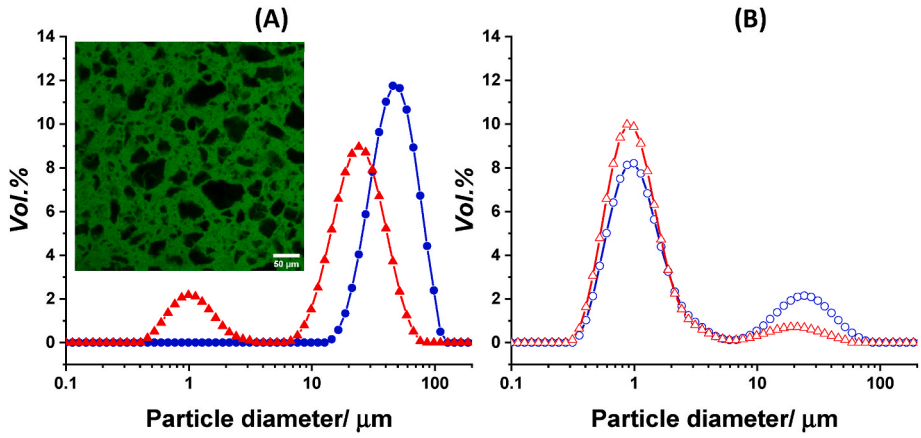

Fig. 1. (A) Particle size distributions (*PSD*) of the coarse *SBPM* particles prepared by rotor-stator mixing: firm (●) and soft (▲). The inset shows a *CLSM* image of firm *SBPM*s that appear black due to negative staining of the background aqueous phase. Scale bar = 50 μm. (B) *PSD*s of the fine *SBPM* suspensions, firm (○) and soft (□), obtained after subjecting the coarse *SBPM* suspensions to the same homogenization conditions as used to form the emulsions (see text).

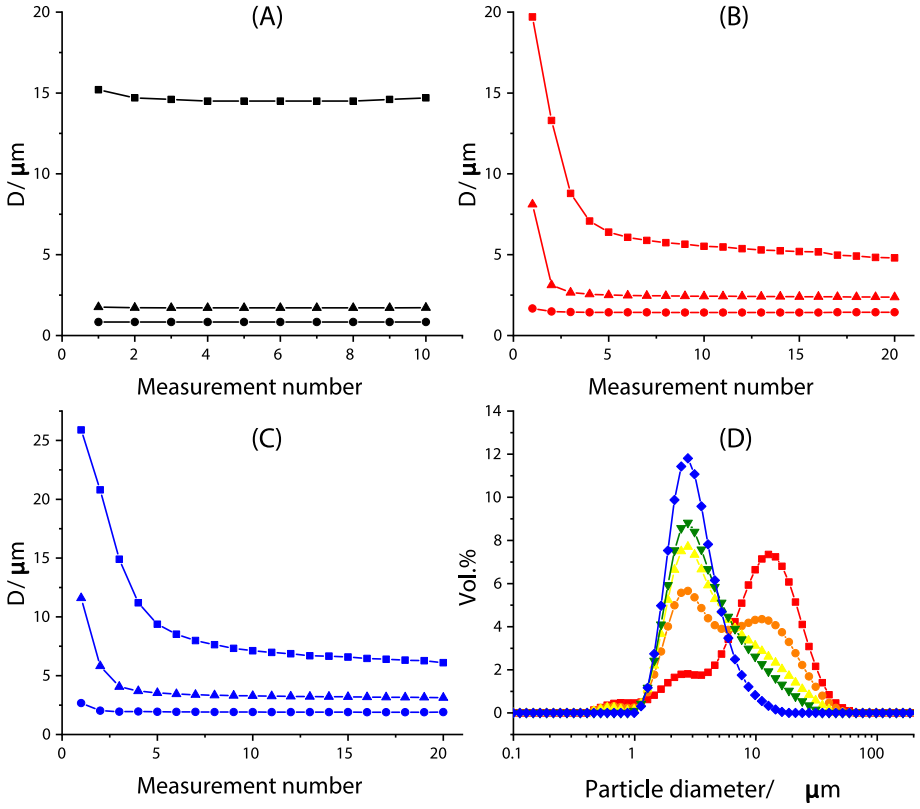

Fig. 2. Evolution of particle size with time after dispersing ϕ_{oil} = 40% emulsions stabilized by (A) native *SBP* (B) soft *SBPM* and (C) firm *SBPM* into the Mastersizer measurement cell. Particle size is represented by the D_{90} (■), D_{50} (▲) and D_{10} (●) values. Each measurement number corresponds to approx. 60 s of data collection. In Fig. 2(D) the volume weighted particle size distributions (PSD) are shown for the emulsions stabilized by the firm *SBPM* shown in Fig. (C) at a measurement numbers 1 (■), 2 (●), 3(▲), 4 (▼) and 20 (◆).

native *SBP* (Fig. 2A), the apparent droplet sizes (D_{90}, D_{50} and D_{10}) were found to be independent of measurement time, suggesting that the emulsions were stable to dilution and not flocculated. In contrast, the droplet sizes of the microgel stabilized emulsions, shown in Figures 2B and C were found to decrease with time, particularly in the case of the larger fractions represented by the D_{90} and D_{50}. We attribute this to weak droplet flocculation. Most of the reduction in particle sizes occurred during the initial 5 to 6 measurements (*i.e.,* 6 ± 2 min), after which the reduction became more gradual, eventually leading to a near plateau value similar to that with the native *SBP*, shown in Fig. 2A.

In Fig. 2D, the volume weighted *PSDs* of the emulsions stabilized by the firm *SBPM* are plotted at various time intervals (*i.e.,* measurement numbers). Initially, the *PSD* suggests a wide distribution of droplet sizes with a major peak centered around 20 µm and a shoulder peak extending to around 1 µm. Over time, apparent droplet sizes are progressively shifted to smaller dimensions, ultimately resulting (*i.e.,* on measurement 20) in a monomodal *PSD* centered between 1 and 10 µm. A similar reduction in (apparent) droplet diameter was observed in the 20 vol% *O/W* emulsions stabilized by *SBPM* (data not shown). From here on, all reported mean droplet sizes for the *SBPM*-stabilized emulsions are based on these 'deflocculated values', *i.e.,* obtained after the *PSD* had stabilized after this continued stirring and calculated by taking an average of at least 5 measurements once the plateau had been established. The results of this analysis are shown for the freshly prepared emulsions in Figures 3A and B for 20 vol% and 40 vol% *O/W* emulsions stabilized by native *SBP*, soft and firm *SBPM*, respectively. For simplicity, we will now refer to these systems using a coding system: 'N' (native *SBP*), 'S' (soft *SPBMG*) and 'F' (firm *SBPM*) followed by a number, either 20 or 40, to represent the emulsion oil volume fraction (20 or 40 vol%), as is shown in Table 2 alongside the corresponding average droplet sizes.

Figures 3A and B suggest a clear influence of the nature of the interfacial species on the particle size distributions. Native *SBP*

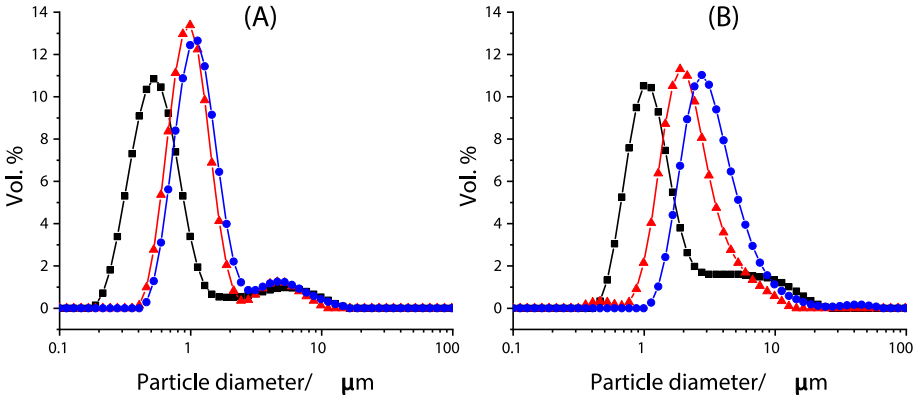

Fig. 3. Particle size distributions of (A) 20 vol% and (B) 40 vol% emulsions stabilized by native *SBP* (■), soft *SBPM* (▲) and firm *SBPM* (●), collected within 2 h of preparation of the emulsions.

Table 2
Average particle sizes of emulsions stabilized by native *SBP* and *SBPM* (after deflocculation) as determined by laser diffraction as a function of storage time. The corresponding % change in particle size between day 1 and day 63 is also shown (ΔD). All particle size measures were significantly different between samples prepared at the same ϕ_{oil} on day 1 and the values of ΔD were significant for all samples ($p < 0.05$).

Size parameter /μm	ϕ_{oil} = 20%			ϕ_{oil} = 40%		
	Native *SBP* N20	Soft *SBPM* S20	Firm *SBPM* F20	Native *SBP* N40	Soft *SBPM* S40″	Firm *SBPM* F40
$D_{3,2}$ Day 1	0.6 ± 0.0	1.1 ± 0	1.2 ± 0	1.3 ± 0.0	2.4 ± 0.0	3.2 ± 0.1
D_{50} Day 1	0.6 ± 0.0	1.1 ± 0	1.2 ± 0	1.3 ± 0.0	2.6 ± 0.0	3.4 ± 0.1
$D_{4,3}$ Day 1	1.2 ± 0.0	1.5 ± 0.01	1.8 ± 0	2.6 ± 0.1	3.1 ± 0.0	4.4 ± 0.3
D_{90} Day 1	2.4 ± 0.1	2.1 ± 0.0	3.2 ± 0.0	6.7 ± 0.2	5.5 ± 0.1	7.7 ± 0.7
$D_{4,3}$ Day 63	4.3 ± 0.0	1.7 ± 0	2.3 ± 0.1	10.5 ± 0.0	3.8 ± 0.1	5.1 ± 0.0
D_{90} Day 63	12.1 ± 0.0	3.0 ± 0.0	5.6 ± 0.3	26.1 ± 0.1	7.7 ± 0.4	9.5 ± 0.1
$\Delta D_{4,3}$/%	257	14	32	301	21	15
ΔD_{90}/%	407	42	77	288	38	24

apparently stabilizes the smallest droplets at both ϕ_{oil} but the *PSD*s appeared bimodal in each case. Fig. 3A shows that for S20 and F20 there was a peak centered at ~1 μm and also a shoulder peak extending to ~20 μm. The latter probably indicates some limited droplet coalescence or flocculation, due to droplets with insufficient interfacial coverage immediately after emulsion preparation (Destribats, Eyharts, et al., 2014). Fig. 3A shows that the softer microgels appeared to be more capable of stabilizing smaller droplets but this was even more apparent at the higher ϕ_{oil} (40%), as seen in Fig. 3B for S40 and F40. These observations are reflected in the average droplet diameters shown in Table 2. For the most part, irrespective of which average is used, the droplet size increases in the order N20 < S20 < F20 and similarly N40 < S40 <F40. The only exception is in the D_{90} values for N20 and N40, which were larger than S20 and S40 respectively.

In the above comparisons, for technological reasons, C_{PTOTAL} in the continuous phase was kept constant at 0.5 wt% for both *SBPM*- and *SBP*-stabilized systems. However, considering each *SBPM* particle as a solvent swollen polymer network, the wt.% particle concentration (C_{SBPM}) can be calculated via Equation (2) and is highest in the soft microgel systems:

$$C_{SBPM}\ (\text{wt.}\%) = 100 \times \text{S} \times \left(\frac{C_{PTOTAL}}{C_{GEL}}\right) \quad (2)$$

This is because the soft parent hydrogels, and therefore each microgel particle derived from it, initially contain more water but also swell to a greater extent when placed in an excess of solvent. The equilibrium swelling ratios (S) for the parent hydrogels, *i.e.,* the increase in mass (and therefore volume, assuming the mass density of gels ≈ that of water) were previously determined to be 1.5 and 1.4 for the soft and firm systems respectively (Stubley et al., 2021). Use of Equation (2) yields C_{SBPM} = 31.3 and 17.5 wt% for the soft and firm *SBPM,* respectively. A higher particle concentration might reasonably be expected to result in smaller oil droplets due to more extensive interfacial coverage and/or a reduction in the extent of 'limited coalescence' during preparation (Destribats, Eyharts, et al., 2014).

As already mentioned, an additional factor affecting the subsequent emulsion stability is that the microgels themselves may undergo some size reduction in the process of homogenizing them with oil, whilst static light scattering cannot distinguish emulsion droplets from microgel particles. Saavedra Isusi, Lohner, et al. (2021) also investigated the breakup of pectin microgel particles during emulsification (Saavedra Isusi, Lohner, et al., 2021). The $D_{3,2}$ of microgels prepared using a rotor-stator mixer was reduced from around 137 μm to 17 μm following high pressure homogenization, although the latter suspensions were suggested to have a "flaky" appearance due to particle aggregation. The 17 μm aggregates were suggested to be assemblies of smaller (around 90 nm) elementary particles. Microgel particles (or aggregates thereof) of different sizes ('small', 'medium' and 'large') were subsequently used to stabilize emulsions. Despite large differences in the initial microgel particle sizes ($D_{3,2}$ = 17 to 137 μm), the $D_{3,2}$ of the resulting emulsions was not significantly different, irrespective of whether emulsions were prepared in a colloid mill or via high pressure homogenization, suggesting the microgels all end up the same in the emulsification process. The $D_{3,2}$ of the resulting oil droplets were also found to be smaller than the $D_{3,2}$ of the initial microgels, which of course is impossible if the same microgels stabilize the droplets. All the above suggests a significant, simultaneous reduction of microgel particle size during emulsion formation. Similar results have been described elsewhere for microgel stabilized emulsions (Lefroy et al., 2021). It is also possible that presence of oil aids the break-up of the larger microgel particles (Saavedra Isusi, Lohner, et al., 2021).

A comparison of the average *SBPM* particle sizes in Table 1 and the overall emulsion particle sizes in Table 2 shows that the *PSD*s of the microgels and resulting emulsions are similar, which also suggests that *SBPM* particle breakdown is modified in the presence of oil. However, in contrast to the work by Saavedra Isusi, Lohner, et al. (2021), the resulting emulsion *PSD*s were significantly different depending on which pectin stabilizer was used (see Table 2). Thus, the average droplet sizes can be tailored by varying ϕ_{oil} and the nature of the stabilizing species, either free polymer or polymer microgel, though whether the variations with microgels are due to the *SBPM* size, their mechanical properties or particle concentration is not clear.

Fig. 4 shows some typical light microscopy images of emulsions for S20 and S40 (Fig. 4A and B), F20 and F40 (Fig. 4C and D), N20 and N40 (Fig. 4E and F) systems. In all images, discrete spherical droplets were observed of sizes in good agreement with the corresponding laser diffraction measurements (Fig. 3). For the N20 and N40 emulsions (Fig. 4E and F), the droplets appeared well dispersed. In contrast, the *SBPM* stabilized emulsions (Fig. 4A–D) appeared to have heterogeneous microstructures, despite samples being diluted and vortex mixed for the preparation of microscope slides. The clusters such as those observed in Fig. 4A–D were presumably flocculated emulsion droplets.

Fig. 5 shows typical *CLSM* images of *undiluted* emulsions at 20x magnification. Oil droplets should appear red due to staining with Nile Red, but for N20 and N40 (Fig. 5A and B, respectively) few discrete droplets can be observed and the images appear almost homogeneously red, due to their small size, making it difficult for the microscope to resolve clearly and compounded by their Brownian motion. The dark spherical regions were air bubbles. For the microgel samples shown in Fig. 5C–F, some clusters of oil droplets are apparent, which appear a brighter shade of red, in agreement with the droplet flocculation in these systems suggested by other techniques. Interestingly, many more dark regions can be seen which, in contrast to Fig. 5A, were clearly non-spherical and therefore unlikely to be air bubbles. These large non-spherical entities are reminiscent of the irregular shaped 'coarse' *SBPM*s shown in the inset of Fig. 1A. They appeared to be more pronounced in emulsions F20 and F40 (Fig. 5E and F) than in S20 and S40 (Fig. 5C and D). Indeed, the particle sizing performed on the fine *SBPM*s shown in Fig. 1B suggests that microgel particles in the size range 10–100 μm can still survive the additional homogenization stage used in emulsion formation and also that this fraction of particles occupies a larger vol% in the firm suspensions compared to the soft suspensions. Thus, there is good evidence for the persistence of large, non-adsorbed microgel particles in the microgel-stabilized emulsions, as also evidenced by the shoulders in the peaks at higher sizes in the PSDs of the emulsions.

To obtain further microstructural information on undiluted

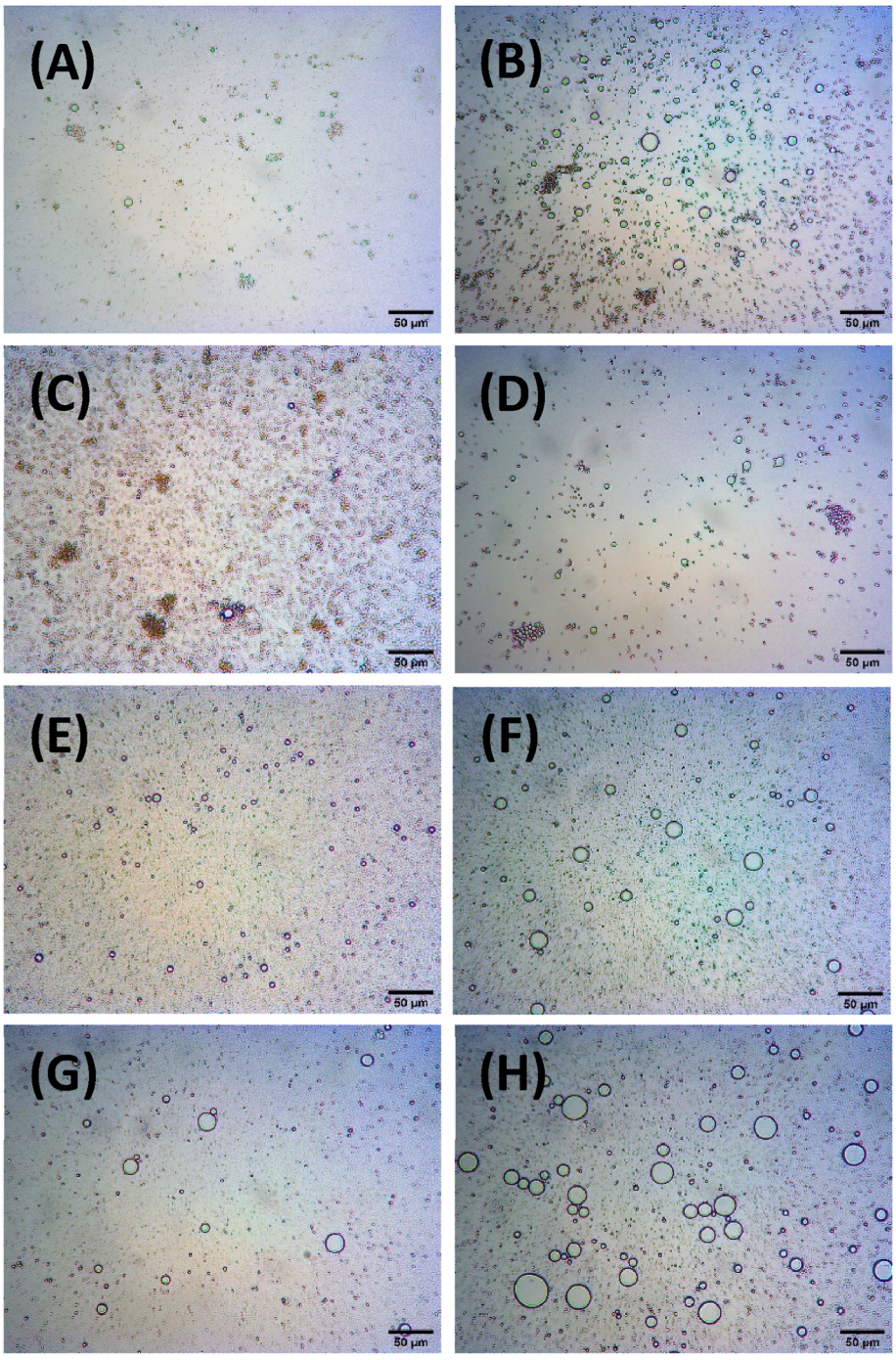

Fig. 4. Typical light microscopy images of diluted emulsions: (A) S20, (B) S40, (C) F20, (D) F40, (E) N20 (F) N40. Images (G) and (H) also show N20 and N40, respectively, after 2 heating and cooling cycles as described in Methods. Scale bar = 50 μm.

emulsions across wider length scales, 40 vol% *O/W* emulsions were investigated via *CRYO-SEM* (Fig. 6). Like the light microscopy and *CLSM* images in Figs. 4 and 5, respectively, emulsions stabilized by native *SBP* (Fig. 6A–C) appeared much more homogeneous, with no apparent flocculation compared to microgel-stabilized emulsions (Fig. 6D–I). The droplets in the latter clearly appeared to be more clustered together and, in some cases, the interfaces between adjacent droplets appeared to have merged, as in bridging flocculation, described below. Unfortunately, the *CRYO-SEM* images did not reveal convincing evidence for the presence of *SBPM* particles at the interface. This was probably due to the lack of contrast between the continuous phase (water) and the water-swollen microgel particles. With hindsight, imaging might have been improved by performing sublimation, which was not done, but this could be attempted in future.

Numerous factors can promote flocculation in particle-stabilized (Pickering) emulsions. For example, flocculation in microgel stabilized emulsions has been studied with respect to the interfacial coverage. Using colloidal poly(N-Isopropylacrylamide) microgel particles as emulsifiers, Destribats, Eyharts, et al. (2014) showed that a low interfacial coverage promotes deformation of microgels adsorbed at the *O/W* interface which in turn leads to an inhomogeneous density distribution of material at the interface. Flocculation originates from droplet bridging via interfacial regions where the microgel density is low or depleted on one droplet and high on another. Consequently, more highly

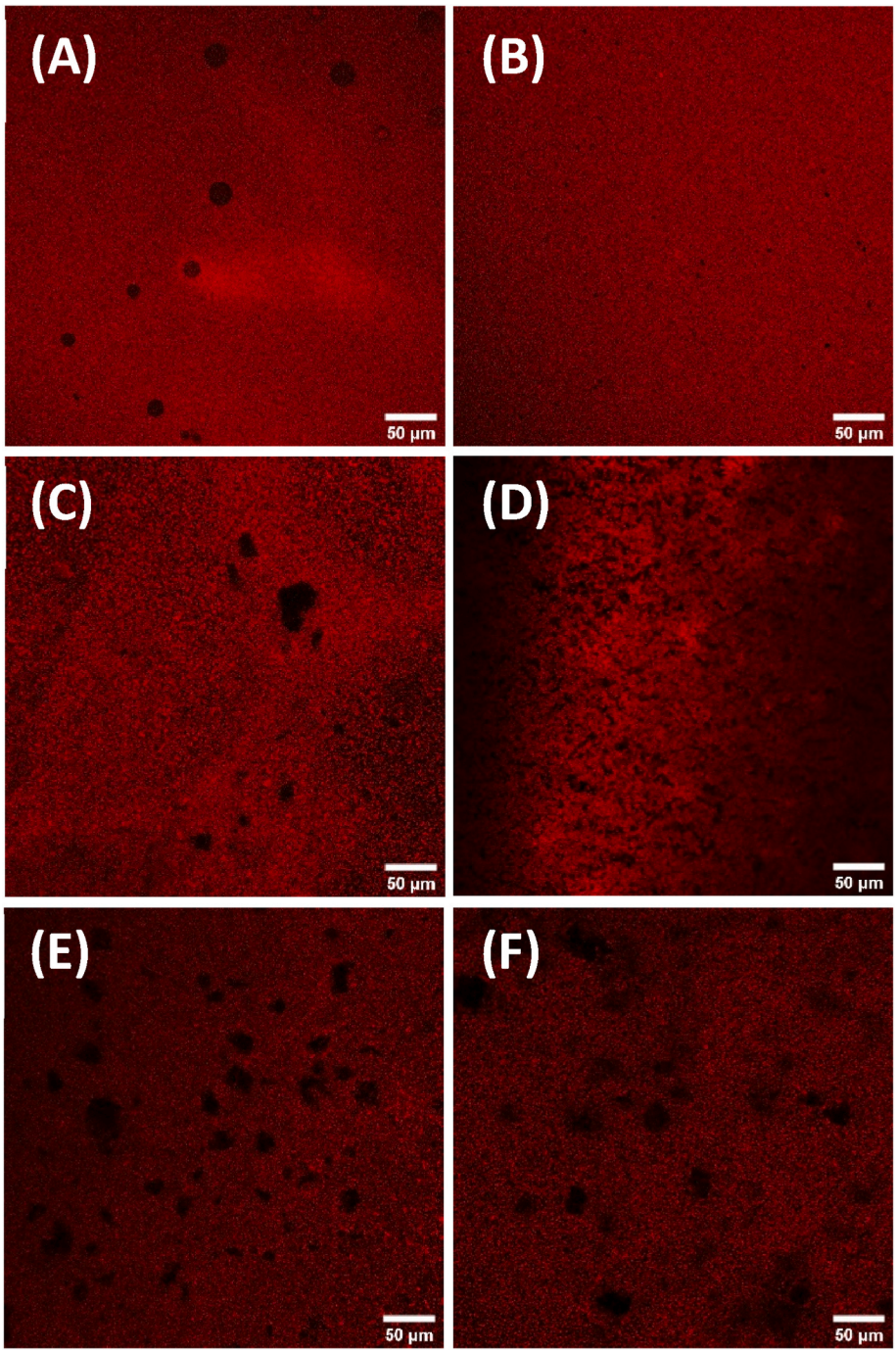

Fig. 5. Typical *CLSM* images of undiluted emulsions: (A) N20, (B) N40, (C) S20, (D) S40, (E) F20 (F) F40. Oil phase stained with Nile Red and appears red. Scale bar = 50 μm. (For interpretation of the references to colour in this figure legend, the reader is referred to the Web version of this article.)

cross-linked (and therefore less deformable) and larger microgel particles, which had a reduced packing efficiency and reduced ability to deform and rearrange at the interface, gave rise to more flocculated emulsions. Such 'bridging monolayers' were visualized by *SEM* and it was suggested that they were still able to prevent extensive droplet coalescence (Destribats, Eyharts, et al., 2014; Destribats, Rouvet, et al., 2014). In contrast, Saavedra Isusi, Lohner, et al. (2021) suggested that an excess of pectin microgel particles could promote flocculation of *O/W* emulsions. For example, at a constant pH (pH 3) and ϕ_{oil} (5%), an increase in the concentration of pectin microgel particles from 0.5 wt% to $>$ 1 wt% led to extensive droplet flocculation (Saavedra Isusi, Weilandt, et al., 2021). The minimum C_{SBPM} used in this study was 10.5 wt% particles in sample F40. Cursory calculations indicate that the number density of *SBPM* particles and size differences between the oil droplets and the *SBPM* are not sufficient for a strong depletion interaction to be responsible for the flocculation. For example, starting with the expression for the depletion energy, V_{depl} (Walstra, 2003), as:

$$V_{depl} = 2\pi R\Pi(2\delta - h)^2 \quad (3)$$

: where δ is the excluded volume thickness, R is the radius of the droplets and Π the osmotic pressure due to the microgel particles in the bulk solution. We then take δ as the minimum possible diameter of the microgel particles as approximately 1 μm, according to values of $D_{3,2}$ in Table 1 for the fine microgels. As a first approximation, the simplest

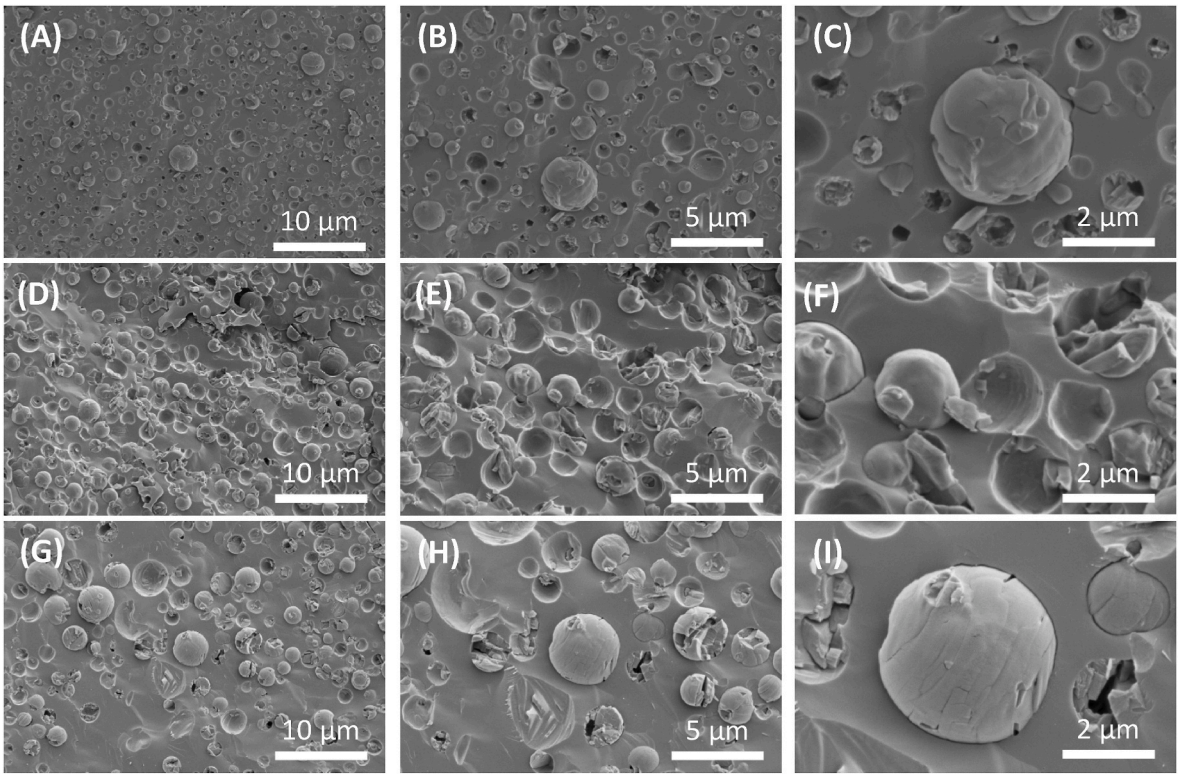

Fig. 6. Typical *CRYO-SEM* images of undiluted emulsions. (A)–(C) = N40, (D)–(F) = S40, (G)–(I) = F40. For left hand side, middle and right hand side images the scale bars are 10, 5 and 2 μm, respectively.

possible expression for $\Pi = Nk_BT$, where N is the number concentration of microgel particles per unit volume, k_B the Boltzmann constant and T the temperature (*i.e.,* no second virial coefficient) may be used. For the firm microgels and the mean droplet surface separation h for $\phi_{oil} = 20$ or 40%, the values of V_{depl} obtained are $<1\ k_BT$ for $R = 2$ μm droplets, (*i.e.,* droplets larger than any $D_{3,2}$ values observed - see Table 2). For the soft microgel–stabilized systems this rises slightly but still $<2\ k_BT$ for $R = 2$ μm droplets.

More experiments are required to elucidate the exact flocculation mechanisms observed in the *SBPM*-stabilized emulsions, however, it should be noted that weak droplet flocculation is not necessarily a disadvantage because it can be used to inhibit droplet movement and creaming and as a result slow down coalescence. Furthermore, tuning droplet-droplet interactions from repulsive to attractive is routinely used to tailor the rheological properties of emulsions (Fuhrmann, Sala, Stieger, & Scholten, 2019) and this was investigated as described in the next section.

3.2. Viscoelasticity of SBP- versus SBPM-stabilized emulsions

In addition to droplet-droplet interactions, emulsion rheology depends strongly on the dispersed phase volume fraction (ϕ) (Fuhrmann et al., 2019; Hermes & Clegg, 2013), which for particle-stabilized emulsions includes the ϕ occupied by both the oil droplets (ϕ_{oil}) and particles (ϕ_{SBPM}). The latter may or may not be adsorbed to droplet interfaces. Fig. 7 shows the shear rate ($\dot{\gamma}$) dependence of the apparent viscosity (η) for all the emulsions studied. Sample N20 showed some evidence for shear thinning from $\dot{\gamma} = 1$ to 100 s^{-1}, before η appeared to plateau at $\eta = 6.37 \pm 0.66$ mPa s between $\dot{\gamma} = 100$ and 1000 s^{-1}. The microgel-stabilized emulsions S20 and F20 were shear thinning over 5 decades in $\dot{\gamma}$ and showed differences in η in the low shear rate region $\dot{\gamma} < 1\ s^{-1}$, with η for S20 being consistently greater than η for F20. The $\dot{\gamma}$ dependent η was similar for these samples beyond 1 s^{-1} but never appeared to plateau or reach the same low value as N20.

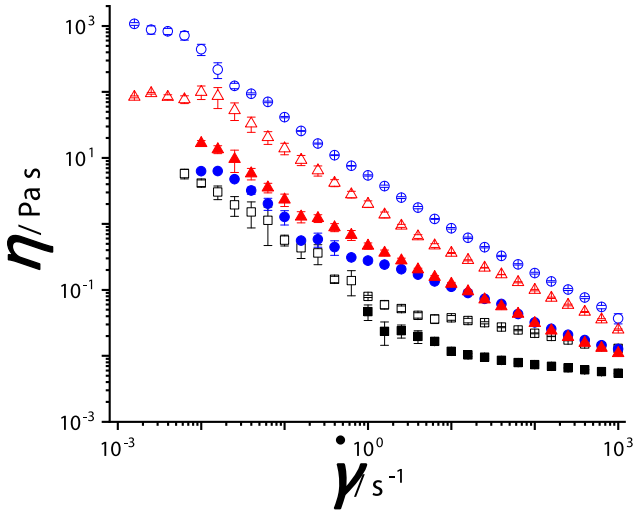

Fig. 7. Apparent viscosity (η) as a function of shear rate ($\dot{\gamma}$) for 20 vol% (filled symbols) and 40 vol% (open symbols) emulsions stabilized by native *SBP* (■), soft *SBPM* (▲) and firm *SBPM* (●).

The higher viscosities of microgel stabilized emulsions compared with the corresponding native *SBP* emulsions can be attributed in most part to the presence of the *SBPM* particles which increases ϕ. Furthermore, droplet flocculation increases the $e\phi$ occupied by the dispersed phase since molecules of the continuous phase become trapped in the interstitial regions of the flocculated emulsion droplets. The more non-spherical (*i.e.,* lower fractal dimension) the clusters become, the greater is this effect (Fuhrmann et al., 2019). The shear induced disruption of such flocs resulted in similar flow curves for F20 and S20 at the higher shear rates investigated. (McClements, 2007; Saavedra Isusi,

Madlindl, et al., 2020; S. Zhang, Holmes, Ettelaie, & Sarkar, 2020).

As expected, the emulsions prepared at ϕ_{oil} = 40% (Fig. 7) also demonstrated shear thinning flow behavior although marked differences were observed compared to the flow curves for the corresponding emulsions prepared at ϕ_{oil} = 20%. For example, at $\dot{\gamma} < 10^{-2}$ s^{-1}, an apparent Newtonian viscosity plateau could be resolved in the microgel stabilized emulsions where η was approximately 100 Pa s for S40 and around an order of magnitude higher in F40. With increasing $\dot{\gamma}$, this plateau was followed by a continuous shear thinning over 5 decades in $\dot{\gamma}$, both samples approaching an η of approximately 0.03–0.05 Pa s at $\dot{\gamma}$ = 1000 s^{-1}. Interestingly, η for F40 was found to be consistently greater than η of S40 over the entire range of $\dot{\gamma}$ investigated, which is the opposite to the trend found for the microgel stabilized emulsions prepared at ϕ_{oil} = 20%. This likely results from differences in the sample microstructure and potentially reflects the rate at which droplet flocs reform following the pre-shear protocol used (see Methods).

Oscillatory shear rheometry was therefore employed to probe the sample microstructure non-destructively. Amplitude sweeps were first performed to define the linear viscoelastic region (*LVER*) where the viscoelastic moduli (*G'* = storage modulus and *G"* = loss modulus) were independent of applied strain (γ). Fig. 8A shows results for the emulsions prepared at ϕ_{oil} = 40%. It can be seen that $G' > G''$ over an extended range in γ, suggesting these emulsions were viscoelastic solids 'at rest'. The G' values vary with the type of sample in the same way as the viscosity does (Fig. 7), that is, G' decreases in the order F40 > S40 > N40. The elasticity must arise from an interconnected droplet structure and the magnitude of G' is related to the number and strength of the inter-droplet interactions (Fuhrmann et al., 2022; Hermes et al., 2013).The length of the *LVER* was similar for *SBPM*-stabilized emulsions, extending to $\gamma \approx 20$ % before the onset of non-linearity and a crossover in G' and G'' was observed at $\gamma \approx 70\%$. Beyond this γ, the emulsions exhibited an essentially liquid-like response (*i.e., G"*>*G'*) implying that the microstructure was irreversibly perturbed. The length of the *LVER* was significantly shorter for N40, characteristic of a more brittle structure than for the *SBPM*-stabilized emulsions (Fuhrmann et al., 2022). The G' and *G"* determined from frequency sweep measurements (Fig. 8B) were in good agreement with the γ sweep measurements. Reliable data could only be collected in a limited frequency range for N40 whereas a plateau in G' extended over several decades in frequency for the *SBPM*-stabilized emulsions, which is again indicative of a more (soft) solid-like structure. Reassuringly, the complex viscosity (η^*) for N40 was in good agreement with the η (Fig. 7), *i.e.,* obeying the Cox-Merz rule, whilst $\eta^* > \eta$ for the *SBPM*-stabilized emulsions but the trend of viscosity for F40 > S40 was maintained.

The emulsions prepared at ϕ_{oil} = 20% were also probed but showed a liquid-like response (*i.e.,* G" > G') (data not shown). Flocculated and concentrated emulsions can demonstrate significant elasticity due to droplet network formation (*i.e.,* emulsion gels) or droplet caging by their nearest neighbors (*i.e.,* soft glassy materials), respectively. Thus, the destruction of droplet networks or cages by external stresses results in a solid-fluid transition (Fuhrmann et al., 2022; Hermes & Clegg, 2013. A more detailed study over a wider range of ϕ_{oil} and ϕ_{SBPM} is required to speculate on the origin of elasticity in these emulsions, but the results suggest that the rheological properties of such emulsions can be tailored through selection of emulsifier, either native *SBP* or *SBPM* of different elasticity.

It is worth noting here that Saavedra Isusi, Madlindl, et al. (2020) began to construct a ternary phase diagram for their pectin microgel stabilized emulsions and suggested that emulsion gel networks were formed above 10 wt% microgel particles even in emulsions prepared at ϕ_{oil} = 10% (Saavedra Isusi, Madlindl, et al., 2020).

Furthermore, *SBP* has previously been added to the continuous phase of *O/W* emulsions and cross-linking initiated to form emulsion filled gels. These systems have been proposed as useful for the microencapsulation and delivery of bioactives (Pan, Li, Meng, Xu, & Zhang, 2021; Zaidel, Chronakis, & Meyer, 2013). Taking inspiration from these studies, one could feasibly use *SBPM* stabilized emulsions for the simultaneous microencapsulation of oil soluble (in the dispersed phase) and water soluble (in the microgels themselves) bioactives. Since the 40 vol% microgel stabilized emulsions demonstrate gel-like rheological properties, but can be made to flow on the application of external stresses (Fig. 8), this may assist in the delivery of such bioactives.

3.3. Physical stability of SBP- versus SBPM-stabilized emulsions

The experimental results discussed so far suggest that native *SBP* is a more efficient emulsifier than *SBPM*s due to its ability to stabilize finer emulsion droplets with no apparent flocculation. However, this does not address the long-term and process stability of the emulsions, which in industry may be subjected to cycles of heating and cooling as well as prolonged storage. Changes in the visual appearance and the *PSD*s of both sets of emulsions were therefore also assessed over at least 9 weeks storage and also after heating and cooling cycles between 75 °C (held at this temperature for 30 min) and 25 °C. The size parameters $D_{4,3}$ and D_{90} are reported, since these are the most sensitive to any droplet coarsening. These were calculated from the emulsion PSDs determined after dilution into the measuring cell, as described in Section 3.1 in relation to Figs. 2–3.

The results of the thermal cycling experiments are illustrated in Figures 9A and B for ϕ_{oil} = 20 and 40%, respectively. It should be noted that none of the emulsions exhibited phase separation as a result of the heating cycles. For the 20 vol% emulsions (Fig. 9A), the histograms show a significant increase in the $D_{4,3}$ and D_{90} after one heating cycle for all samples, compared to the initial non-heated emulsions. A further increase in size between the 1st and 2nd heating cycle was significant for all samples - with the exception of the $D_{4,3}$ for S20. For the 40 vol% emulsions (Fig. 9B), the increases in droplet size for N40 were significant but the *SBPM*-stabilized emulsions (S40 and F40) appeared to be more

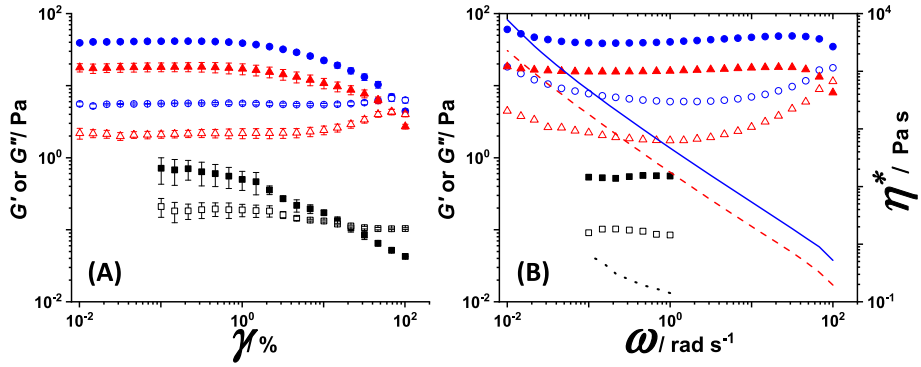

Fig. 8. G' = storage modulus (filled symbols), G" = loss modulus (open symbols) as a function of: (A) strain amplitude (γ) and (B) angular frequency (ω) for emulsions N40 (■), S40 (▲) and F40 (●). In (B), the lines show the complex viscosity (η^*) of N40 (dotted line), S40 (dashed line) and F40 (solid line).

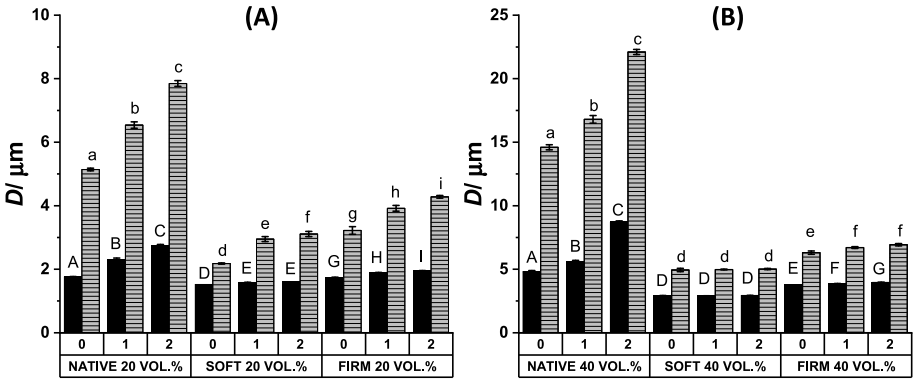

Fig. 9. Average particle diameters (D) of emulsions represented by the $D_{4,3}$ (dotted columns) and D_{90} (striped columns) values before (0) and after one (1) or two (2) heating cycles as described in the text. (A) and (B) show results for ϕ_{oil} = 20 vol% and 40 vol%, respectively, stabilized by native *SBP*, soft *SBPM* or firm *SBPM*. Columns sharing the same letters do not show significant differences between the heating cycles ($p < 0.05$) - upper case letters being are used to indicate this for the $D_{4,3}$ values and lowercase letters are used for the D_{90} values.

stable to heating. For example, no significant differences were found in $D_{4,3}$ or D_{90} of S40 after two heating cycles. Furthermore, the D_{90} for F40 increased significantly after the first heating cycle but the increase after the 2nd heating cycle was not significant. The use of softer microgels for emulsion stabilization has been shown to lead to an increased interfacial elasticity (Huang et al., 2021; Li et al., 2015) and heating would be expected to soften the *SBPM* particles further, further improving the stability of droplets against coalescence under these conditions.

The average droplet sizes and percentage increases in the droplet diameter (ΔD) after two heating cycles are shown in Table 3. The ΔD was found to be highest for the *SBP*-stabilized emulsions irrespective of ϕ_{oil}. For example, the $D_{4,3}$ of N20 and N40 increased from 1.76 to 2.74 µm and from 4.8 to 8.7 µm, respectively, corresponding to large ΔD of 55.7 and 81.3%, respectively. This is hypothesized as being due to the non-Pickering nature of the *SBP* stabilizer compared to the *SBPM*, which is therefore less able to prevent coalescence and Ostwald ripening. To confirm this hypothesis, light microscopy was also performed on these emulsions after 2 heating cycles and typical results are shown in Figures 4G and H for N20 and N40, respectively. Compared to the corresponding *unheated* samples (shown in Fig. 4E and F), a clear increase in droplet size is apparent but with the absence of extensive droplet flocculation. No conclusive differences were observed in the light microscopy images (not shown) of any of the *SBPM*-stabilized emulsions after heating, despite significant increases in the apparent droplet sizes measured by laser diffraction for all samples except S40. However, it should be remembered that the samples were extensively diluted before the light microscopy, which might have disrupted any loose flocs of droplets, whilst the *PSD*s and resultant droplet size measurements may be skewed by a small number of some persistent large flocs (Fig. 2), which may possibly be strengthened by heating. The *SBPM*-stabilized emulsions at ϕ_{oil} = 40% were more stable against heat-induced droplet coarsening compared to those at ϕ_{oil} = 20% (Table 3). This suggests an additional contribution to emulsion stability from the higher ϕ_{SBPM} and its effect on the viscoelasticity of the emulsions, as discussed above.

Fig. 10 shows the evolution of particle size with storage time at 25 °C of the non-heated emulsions. Figures 10A and C shows the D_{90} and $D_{4,3}$ for emulsions with ϕ_{oil} = 20%, respectively, whilst Figures 10B and D shows the corresponding D_{90} and $D_{4,3}$ for emulsions with ϕ_{oil} = 40%. The data presented illustrate a profound difference between the stability of emulsions stabilized by native *SBP* and that of the *SBPM*-stabilized emulsions. The sizes in the latter remain more or less constant over 63 days storage, whereas the droplet sizes (Fig. 10B and D) in the N40 emulsion appear to increase progressively and continuously over at least 56 days, before beginning to plateau off. The same behavior was observed in the N20 system (Fig. 10A and C), although there was slightly more scatter in the data and no clear evidence for a plateau in size at the end of the storage period. Table 2 shows the D_{90} and $D_{4,3}$ for each emulsion on day 1 and day 63 and the ΔD over this storage period. In all cases, the increase in droplet size was significant but ΔD was substantially lower for the *SBPM*-stabilized emulsions. For example, the $D_{4,3}$ for N40 increased by 301% compared to an increase of 21% and 15% for S40 and F40 respectively.

At the C_{PTOTAL} (0.5 wt%) used here, the native *SBP* is clearly a poor stabilizer under temperature cycling and prolonged storage conditions. Other authors have previously suggested that although the protein side chains anchor strongly to the oil-water interface, the polysaccharide chains of *SBP* protruding into the continuous phase are insufficient to confer effective steric stabilization. (Any ionized non-methylated *GalA* residues will also confer additional electrostatic repulsion). Indeed, the stability of *SBP*-based emulsions has been improved by chemical cross-linking of *SBP* (Jung & Wicker, 2012; Zhang et al., 2015) in dilute solution to increase the *MW* before their use as emulsifiers, as noted in the Introduction. In a similar vein, protein side chains of *SBP* have been used as a target for chemical crosslinking via lysine residues in a reaction catalyzed by genipin (Lin, Yu, Ai, Zhang, & Guo, 2020). Such supramolecular aggregates could also be regarded as microgel particles, but are likely to be substantially 'softer' than those presented here. Nonetheless, in all of these studies, droplet coarsening on storage was reduced for modified *SBP* stabilized emulsions compared to the non-cross-linked controls (Jung & Wicker, 2012; Lin, Yu, Ai, Zhang, & Guo, 2020), even at elevated temperatures (60 °C) (L. Zhang et al., 2015).

Most of the emulsions were found to undergo phase separation into a droplet rich cream layer and a droplet depleted serum layer on prolonged storage, as illustrated by the photographs in Fig. 11A and B for the 20 vol% emulsions and 11C-D for the 40 vol% emulsions on day 1 and day 21. This gravitational separation was quantified by the creaming index (*CI*) given by Equation (1). For the 20 vol% emulsions

Table 3
Average particle sizes of emulsions stabilized by native *SBP* and *SBPM* (after deflocculation) as determined by laser diffraction as a function of heating and cooling cycles. The % change in droplet size (ΔD) after two heating cycles is shown in final 2 columns.

Sample	Before heating		After 1 heating cycle		After 2 heating cycles		%ΔD after 2 heating cycles	
	$D_{4,3}$/ µm	D_{90}/ µm	$D_{4,3}$/ µm	D_{90}/ µm)	$D_{4,3}$/ µm	D_{90}/ µm)	$\Delta D_{4,3}$	ΔD_{90}
N20	1.8 ± 0.0	5.1 ± 0.0	2.3 ± 0.1	6.5 ± 0.1	2.7 ± 0.0	7.9 ± 0.1	55.7	52.7
S20	1.5 ± 0	2.2 ± 0.0	1.6 ± 0.0	3.0 ± 0.1	1.6 ± 0.0	3.1 ± 0.1	4.6	42.7
F20	1.7 ± 0.03	3.2 ± 0.1	1.9 ± 0.0	3.9 ± 0.1	2.0 ± 0.0	4.3 ± 0.0	13.4	32.9
N40	4.9 ± 0.1	14.6 ± 0.2	5.6 ± 0.1	16.8 ± 0.3	8.7 ± 0.1	22.1 ± 0.2	81.3	51.4
S40	2.9 ± 0.0	4.9 ± 0.1	2.9 ± 0.1	5.0 ± 0.0	2.9 ± 0.0	5.0 ± 0.1	0.3	1.4
F40	3.7 ± 0.0	6.3 ± 0.1	3.9 ± 0.0	6.7 ± 0.1	4.0 ± 0.0	6.9 ± 0.1	5.9	9.8

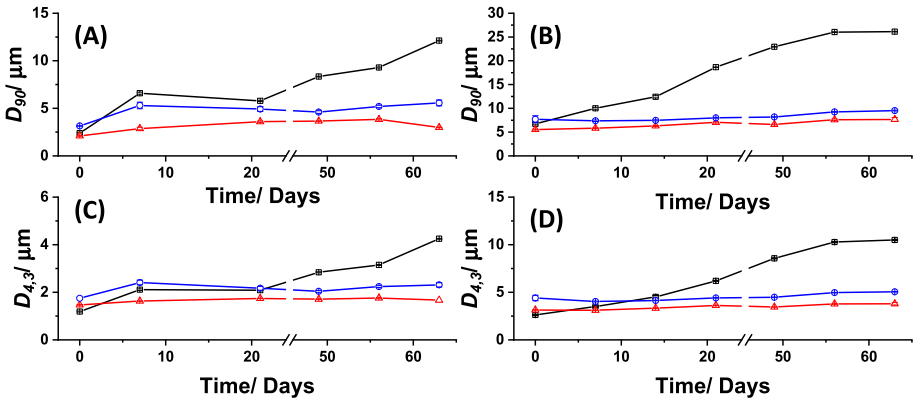

Fig. 10. Evolution of (A) D_{90} and (B) $D_{4,3}$ with prolonged storage time at 25 °C for the $\phi_{oil} = 20$ vol% emulsions stabilized by native *SBP* (■), soft *SBPM* (▲) and firm *SBPM* (●). (B) and (D) show the corresponding D_{90} and $D_{4,3}$ values for the $\phi_{oil} = 40$ vol% emulsions. Lines through the points are to guide the eye.

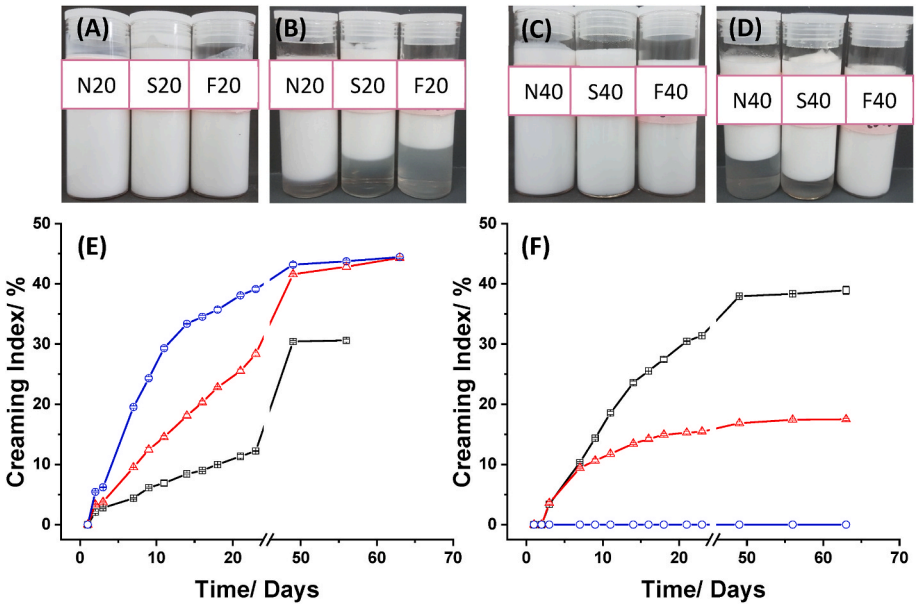

Fig. 11. Visual assessment of creaming stability for emulsions on prolonged storage at 25 °C. (A) and (B) show photographs of 20 vol% emulsions on day 1 and day 21 respectively. (C) and (D) shows photographs of 40 vol% emulsions on day 1 and day 21 respectively. Each left, middle and right photograph shows emulsions were stabilized by native *SBP*, soft and firm *SBPM* microgels. (E) and (F) show the creaming index at various time intervals over 63 days storage for 20 vol% and 40 vol% emulsions, respectively, stabilized by native *SBP* (■), soft *SBPM* (▲) and firm *SBPM* (●). Lines through the points are to guide the eye.

(Fig. 11E), the rate and extent of creaming over the initial 21 days storage followed the order F20 > S20 > N20. By day 49 creaming in S20 appeared to have accelerated and approached the *CI* of F20. The remaining 2 weeks showed a reduced rate of creaming for the *SBPM*-stabilized emulsions, which reached a similar *CI* of ~44% on day 63. The cream layer in N20 was accidently disrupted after measuring the *CI* on day 56, although the *CI* already appeared to be approaching a plateau of CI ≈ 30.5%.

The observed trend in creaming stability was reversed for the 40 vol % emulsions with N40 > S40 > F40, clearly visible in the corresponding photographs (Fig. 11A–D). Sample F40 showed no evidence for creaming over the entire storage period. The *CI* of N40 and S40 appeared to have plateaued at around day 49. Taking an average of the final 3 data points gives *CI* = 38.4 ± 0.4% and 17.3 ± 0.3% for N40 and S40, respectively (Fig. 11F). Hence, S40 creamed to a lesser extent than S20, whereas N40 creamed more extensively than N20.

For the *SBP*-stabilized emulsions, the time dependence of the *CI* is well correlated with the progressive increase in droplet size over the same storage period (see Fig. 10A and C and Table 1) according to Stokes' Law, which can also explain the relatively faster and more extensive creaming of S20 and F20 compared to N20 if the flocculation increases the effective droplet size but does not lead to a droplet gel network entirely preventing creaming (Hermes et al., 2013). Indeed, the improved stability to creaming of the *SBPM*-stabilized emulsions at the higher ϕ_{oil} of 40% is probably related to the development of this sort of interconnected microstructure, as suggested by the oscillatory shear rheometry results (Fig. 8).

4. Conclusions

In this work we have introduced a novel route to improved emulsion stability by converting *SBP*, a surface active hydrocolloid, into *SBP* microgel particles (*SBPM*). Native *SBP* was found to be the most efficient emulsifier, giving the smallest average droplet sizes. However, owing to the Pickering emulsification mechanism, the *SBPM*-stabilized emulsions demonstrated improved stability towards droplet coarsening on (i) temperature cycling and (ii) prolonged storage at ambient temperature compared to native *SBP* at the same total *SBP* content. Furthermore, the use of *SBPMs* as emulsifiers enabled significant enhancement of the viscoelasticity of the emulsions, due to a combination of droplet flocculation and the increase in overall volume faction of dispersed particles due to the *SBPM* themselves. The softer *SBPM* seemed to give slightly smaller initial droplet sizes than the firm *SBPM*, but the latter seemed to lead to greater thickening effects, particularly at higher volume fractions of oil droplets, that even more significantly curtailed creaming. Our future work on these systems will aim to investigate separately the

influence of ϕ_{oil} and ϕ_{SBPMG} on the properties of such emulsions and also investigate a wider range particle of elasticities, with the mechanical properties of individual particles also assessed (*e.g.,* via atomic force microscopy). Considering the great potential for *SBPMs* as emulsifiers in foods, their emulsifying properties should also be investigated under different environmental conditions, for example, by varying the ionic strength and pH and also with food-grade oils.

Author contributions

Samuel J. Stubley: Conceptualization, Methodology, Investigation, Formal analysis, Writing – original draft. **Olivier J. Cayre**: Conceptualization, Writing – review & editing, Supervision. **Brent S. Murray**: Conceptualization, Visualization, Writing – review & editing, Supervision. **Isabel Celigueta Torres:** Conceptualization, Review & editing.

Declaration of competing interest

There are no conflicts to declare.

Data availability

Data will be made available on request.

Acknowledgements

We acknowledge and thank Dr. Isabel Fernández Farrés for her support and input into this work during her time at Nestlé. We thank Mr. Stuart Micklethwaite of the Leeds electron microscopy and spectroscopy center and Dr. Ruth Hughes of the Leeds bio-imaging and flow cytometry facility for their excellent technical assistance in sample imaging via *SEM* and *CLSM* respectively. SJS gratefully acknowledges the Engineering and Physical Sciences Research Council (EPSRC) funded Centre for Doctoral Training in Soft Matter and Functional Interfaces (SOFI), Grant Ref. No. EP/L015536/1 as well as Nestlé PTC Confectionery (York, UK) for financial support.

References

Adams, S., Frith, W. J., & Stokes, J. R. (2004). Influence of particle modulus on the rheological properties of agar microgel suspensions. *Journal of Rheology, 48*, 1195–1213.

Akhtar, M., Dickinson, E., Mazoyer, J., & Langendorff, V. (2002). Emulsion stabilizing properties of depolymerized pectin. *Food Hydrocolloids, 16*(3), 249–256.

Alba, K., & Kontogiorgos, V. (2017). Pectin at the oil-water interface: Relationship of molecular composition and structure to functionality. *Food Hydrocolloids, 68*, 211–218.

Atarés, L., Marshall, L. J., Akhtar, M., & Murray, B. S. (2012). Structure and oxidative stability of oil in water emulsions as affected by rutin and homogenization procedure. *Food Chemistry, 134*(3), 1418–1424.

Bunzel, M. (2010). Chemistry and occurrence of hydroxycinnamate oligomers. *Phytochemistry Reviews, 9*(1), 47–64.

Chen, H., Qiu, S., Gan, J., Liu, Y., Zhu, Q., & Yin, L. (2016). New insights into the functionality of protein to the emulsifying properties of sugar beet pectin. *Food Hydrocolloids, 57*, 262–270.

Dea, I. C. M., & Madden, J. K. (1986). Acetylated pectic polysaccharides of sugar beet. *Food Hydrocolloids, 1*(1), 71–88.

Destribats, M., Eyharts, M., Lapeyre, V., Sellier, E., Varga, I., Ravaine, V., et al. (2014a). Impact of pNIPAM microgel size on its ability to stabilize pickering emulsions. *Langmuir, 30*(7), 1768–1777.

Destribats, M., Rouvet, M., Gehin-Delval, C., Schmitt, C., & Binks, B. P. (2014b). Emulsions stabilised by whey protein microgel particles: Towards food-grade pickering emulsions. *Soft Matter, 10*(36), 6941–6954.

Dickinson, E. (2003). Hydrocolloids at interfaces and the influence on the properties of dispersed systems. *Food Hydrocolloids, 17*(1), 25–39.

Dickinson, E. (2015). Microgels — an alternative colloidal ingredient for stabilization of food emulsions. *Trends in Food Science & Technology, 43*(2), 178–188.

Dickinson, E. (2016). Exploring the frontiers of colloidal behaviour where polymers and particles meet. *Food Hydrocolloids, 52*, 497–509.

Ellis, A., & Jacquier, J. C. (2009). Manufacture and characterisation of agarose microparticles. *Journal of Food Engineering, 90*(2), 141–145.

Fuhrmann, P. L., Breunig, S., Sala, G., Sagis, L., Stieger, M., & Scholten, E. (2022). Rheological behaviour of attractive emulsions differing in droplet-droplet interaction strength. *Journal of Colloid and Interface Science, 607*, 389–400.

Fuhrmann, P. L., Sala, G., Stieger, M., & Scholten, E. (2019). Clustering of oil droplets in o/w emulsions: Controlling cluster size and interaction strength. *Food Research International, 122*, 537–547.

Funami, T., Zhang, G., Hiroe, M., Noda, S., Nakauma, M., Asai, I., et al. (2007). Effects of the proteinaceous moiety on the emulsifying properties of sugar beet pectin. *Food Hydrocolloids, 21*(8), 1319–1329.

Hermes, M., & Clegg, P. S. (2013). Yielding and flow of concentrated Pickering emulsions. *Soft Matter, 9*(31), 7568–7575.

Huang, P., Huang, C., Ma, X., Gao, C., Sun, F., Yang, N., et al. (2021). Effect of pH on the mechanical, interfacial, and emulsification properties of chitosan microgels. *Food Hydrocolloids, 121*, Article 106972.

Hu, M., Wu, Y., Wang, J., Lu, W., Gao, Z., Xu, L., et al. (2021). Emulsions stabilization and lipid digestion profiles of sodium alginate microgels: Effect of the crosslink density. *Food Biophysics, 16*(3), 346–354.

Ishii, T., Matsumiya, K., Aoshima, M., & Matsumura, Y. (2018). Microgelation imparts emulsifying ability to surface-inactive polysaccharides—bottom-up vs top-down approaches. *Npj Science of Food, 2*(1), 15.

Jung, J., & Wicker, L. (2012). Laccase mediated conjugation of sugar beet pectin and the effect on emulsion stability. *Food Hydrocolloids, 28*(1), 168–173.

Kargar, M., Fayazmanesh, K., Alavi, M., Spyropoulos, F., & Norton, I. T. (2012). Investigation into the potential ability of Pickering emulsions (food-grade particles) to enhance the oxidative stability of oil-in-water emulsions. *Journal of Colloid and Interface Science, 366*(1), 209–215.

Khalighi, S., Berger, R. G., & Ersoy, F. (2020). Cross-linking of fibrex gel by fungal laccase: Gel rheological and structural characteristics. *Processes, 8*(1).

Kirby, A. R., MacDougall, A. J., & Morris, V. J. (2006). Sugar beet pectin–protein complexes. *Food Biophysics, 1*(1), 51.

Lefroy, K. S., Murray, B. S., Ries, M. E., & Curwen, T. D. (2021). A natural, cellulose-based microgel for water-in-oil emulsions. *Food Hydrocolloids, 113*, Article 106408.

Leroux, J., Langendorff, V., Schick, G., Vaishnav, V., & Mazoyer, J. (2003). Emulsion stabilizing properties of pectin. *Food Hydrocolloids, 17*(4), 455–462.

Levigne, S.b. V., Ralet, M.-C. J., Quéméner, B. C., Pollet, B. N. L., Lapierre, C., & Thibault, J.-F. o. J. (2004). Isolation from sugar beet cell walls of arabinan oligosaccharides esterified by two ferulic acid monomers. *Plant Physiology, 134*(3), 1173–1180.

Li, Z., Harbottle, D., Pensini, E., Ngai, T., Richtering, W., & Xu, Z. (2015). Fundamental study of emulsions stabilized by soft and rigid particles. *Langmuir, 31*(23), 6282–6288.

Lin, J., Yu, S., Ai, C., Zhang, T., & Guo, X. (2020). Emulsion stability of sugar beet pectin increased by genipin crosslinking. *Food Hydrocolloids, 101*, Article 105459.

Lyon, L. A., & Fernandez-Nieves, A. (2012). The polymer/colloid duality of microgel suspensions. *Annual Review of Physical Chemistry, 63*(1), 25–43.

McClements, D. J. (2007). Critical review of techniques and methodologies for characterization of emulsion stability. *Critical Reviews in Food Science and Nutrition, 47*(7), 611–649.

Mironov, M. A., Shulepov, I. D., Ponomarev, V. S., & Bakulev, V. A. (2013). Synthesis of polyampholyte microgels from colloidal salts of pectinic acid and their application as pH-responsive emulsifiers. *Colloid and Polymer Science, 291*(7), 1683–1691.

Murray, B. S. (2019). Microgels at fluid-fluid interfaces for food and drinks. *Advances in Colloid and Interface Science, 271*, Article 101990.

Ngouémazong, E. D., Christiaens, S., Shpigelman, A., Van Loey, A., & Hendrickx, M. (2015). The emulsifying and emulsion-stabilizing properties of pectin: A review. *Comprehensive Reviews in Food Science and Food Safety, 14*(6), 705–718.

Pan, Y., Li, X.-M., Meng, R., Xu, B.-C., & Zhang, B. (2021). Investigation of the formation mechanism and curcumin bioaccessibility of emulsion gels based on sugar beet pectin and laccase catalysis. *Journal of Agricultural and Food Chemistry, 69*(8), 2557–2563.

Saavedra Isusi, G. I., Bindereif, B., Karbstein, H. P., & van der Schaaf, U. S. (2020). Polymer or microgel particle: Differences in emulsifying properties of pectin as microgel or as individual polymer chains. *Colloids and Surfaces A: Physicochemical and Engineering Aspects, 598*, Article 124793.

Saavedra Isusi, G. I., Karbstein, H. P., & van der Schaaf, U. S. (2019). Microgel particle formation: Influence of mechanical properties of pectin-based gels on microgel particle size distribution. *Food Hydrocolloids, 94*, 105–113.

Saavedra Isusi, G. I., Lohner, N., Karbstein, H. P., & van der Schaaf, U. S. (2021). Emulsions stabilised with pectin-based microgels: Investigations into the break-up of droplets in the presence of microgels. *Journal of Food Engineering, 294*, Article 110421.

Saavedra Isusi, G. I., Madlindl, L. B., Karbstein, H. P., & van der Schaaf, U. S. (2020). Microstructures and conformational arrangement in emulsions caused by concentration ratios of pectin-based microgels and oil. *Colloids and Surfaces A: Physicochemical and Engineering Aspects, 602*, Article 125166.

Saavedra Isusi, G. I., Weilandt, M., Majollari, I., Karbstein, H. P., & van der Schaaf, U. S. (2021). Emulsions stabilised with pectin-based microgels: Investigations into the effect of pH and ionic strength on emulsion stability. *Food & Function, 12*(16), 7227–7238.

Sarkar, A., Zhang, S., Holmes, M., & Ettelaie, R. (2019). Colloidal aspects of digestion of Pickering emulsions: Experiments and theoretical models of lipid digestion kinetics. *Advances in Colloid and Interface Science, 263*, 195–211.

Schmidt, U. S., Schmidt, K., Kurz, T., Endreß, H. U., & Schuchmann, H. P. (2015). Pectins of different origin and their performance in forming and stabilizing oil-in-water-emulsions. *Food Hydrocolloids, 46*, 59–66.

Siew, C. K., & Williams, P. A. (2008). Role of protein and ferulic acid in the emulsification properties of sugar beet pectin. *Journal of Agricultural and Food Chemistry, 56*(11), 4164–4171.

Stubley, S. J., Cayre, O. J., Murray, B. S., & Torres, I. C. (2022). Pectin-based microgels for rheological modification in the dilute to concentrated regimes. *Journal of Colloid and Interface Science, 628*, 684–695.

Stubley, S. J., Cayre, O. J., Murray, B. S., Torres, I. C., & Farrés, I. F. (2021). Enzyme cross-linked pectin microgel particles for use in foods. *Food Hydrocolloids, 121*, Article 107045.

Thakur, B. R., Singh, R. K., Handa, A. K., & Rao, M. A. (1997). Chemistry and uses of pectin — a review. *Critical Reviews in Food Science and Nutrition, 37*(1), 47–73.

Thibault, J.-F., Garreau, C., & Durand, D. (1987). Kinetics and mechanism of the reaction of ammonium persulfate with ferulic acid and sugar-beet pectins. *Carbohydrate Research, 163*(1), 15–27.

Walstra, P. (2003). Colloidal interactions. In *Physical chemistry of foods* (1st ed.). USA: Marcel Dekker.

Williams, P. A., Sayers, C., Viebke, C., Senan, C., Mazoyer, J., & Boulenguer, P. (2005). Elucidation of the emulsification properties of sugar beet pectin. *Journal of Agricultural and Food Chemistry, 53*(9), 3592–3597.

Yapo, B. M., Robert, C., Etienne, I., Wathelet, B., & Paquot, M. (2007). Effect of extraction conditions on the yield, purity and surface properties of sugar beet pulp pectin extracts. *Food Chemistry, 100*(4), 1356–1364.

Zaidel, D. N. A., Chronakis, I. S., & Meyer, A. S. (2013). Stabilization of oil-in-water emulsions by enzyme catalyzed oxidative gelation of sugar beet pectin. *Food Hydrocolloids, 30*(1), 19–25.

Zhang, S., Holmes, M., Ettelaie, R., & Sarkar, A. (2020). Pea protein microgel particles as Pickering stabilisers of oil-in-water emulsions: Responsiveness to pH and ionic strength. *Food Hydrocolloids, 102*, Article 105583.

Zhang, L., Shi, Z., Shangguan, W., Fang, Y., Nishinari, K., Phillips, G. O., et al. (2015). Emulsification properties of sugar beet pectin after modification with horseradish peroxidase. *Food Hydrocolloids, 43*, 107–113.